Multiple-Scattering Effects in EXAFS Spectroscopy of Oxygen-Bridged Iron Complexes. Possibility of Angle Determination by EXAFS Analysis

Man Sung Co,[1a] Wayne A. Hendrickson,[1b] Keith O. Hodgson,*[1a] and Sebastian Doniach[1c]

Contribution from the Departments of Chemistry and Applied Physics, Stanford University, Stanford, California 94305, and the Laboratory for the Structure of Matter, Naval Research Laboratory 6030, Washington, D.C. 20375. *Received June 21, 1982*

Abstract: The Fe–Fe EXAFS in X-ray absorption data measured from a series of 12 oxygen-bridged iron complexes has been analyzed to investigate systematically the effect of intervening atoms on the structural information derived from EXAFS analysis. The series includes dihydroxo- or dialkoxo-bridged dimers and μ-oxo-bridged dimers and trimers. Three major pathways are considered for a photoelectron to travel to and from an absorber A to a scatterer C in a bridged A–B–C system. Pathway I is the direct backscattering from A to C and back. Pathway II is the multiple-scattering path via atom B in either the outgoing or the incoming trip. Pathway III is the multiple-scattering path via atom B in both outgoing and incoming trips. When the A–B–C (as exemplified by Fe–O–Fe) bridging angle is small, e.g., ca. 100°, the three pathways are resolvable in the Fourier transform and can be analyzed independently. A constant phase shift of approximately π and a linear phase shift of −0.11 Å are found as the photoelectron propagates each time through the potential of the bridging oxygen atom. When the bridging angle is large, greater than ca. 150°, the pathway III will become dominant. This pathway is signified by an amplitude enhancement that is found to correlate with the bridging angle, a result of the angular dependence of forward scattering. Angle determination becomes possible from analyzing this multiple-scattering pathway. Fe–Fe interatomic distance can also be calculated to an accuracy of ±0.05 Å.

Extended X-ray absorption fine structure (EXAFS) spectroscopy has become a useful technique for investigating the local coordination environment of specific atomic species in complex chemical systems. Although the method is only sensitive to short-range order (distances within about 4 Å of the absorber), it has the advantage of focusing on particular atoms and of being applicable to any physical state including liquid solutions and amorphous solids. Advances in the development of theory, coupled with high-quality data, now allow the technique to determine interatomic distances with high accuracy (usually within ±0.02 Å) for the first coordination shell about an absorbing atom and to assign with less accuracy the coordination number and identity of the ligating atoms. A particularly important area of EXAFS applications has been to metalloproteins, since metal sites often correspond to the centers of biological activity in proteins. Several such studies have provided valuable information about the structure of the first coordination shell around the metal sites. However, studies beyond the first coordination sphere have met with less success. This paper addresses this problem by exploring experimentally the consequences of intervening atoms between the absorber and scatterer which render the short-range one-electron single-scattering EXAFS theory inadequate.

The multiple-scattering atom effect in EXAFS was first observed when theoretical calculations of EXAFS were compared with measurements on copper metal.[2] The observed amplitude of the scattered wave for the fourth copper shell was larger than the amplitude calculated from the single-scattering theory, and the observed phase shift was also off by approximately π from the calculated phase shift. These discrepancies were explained as an effect of first-shell atoms that intervene directly in the absorber-to-scatterer path to the fourth-shell atoms in the face-centered cubic lattice. Rather than occluding the EXAFS from the fourth-shell atoms as might naively be expected, the intervening atoms actually accentuate the EXAFS due to the shadowed atoms by enhanced forward scattering of both the outgoing and the backscattered photoelectron waves. These multiple-scattering events also cause additional phase shifts. Multiple-scattering effects have also been observed in many inorganic π-acceptor complexes, where di- or triatomic ligands (e.g., CO, CN^-, NCS^-) are linearly bound to the X-ray absorbing transition metal. For example, in $[Mo(NCS)_6]^{3-}$ the amplitude of the carbons and sulfurs of the isothiocyanate ligands are distinctly enhanced in the Fourier transform spectrum.[3] In the case of $Mo(CO)_6$ the amplitude of the second oxygen shell is even larger than that of the first carbon shell.[3] Recently, a multiple-scattering formulation has been developed by Teo to extract interatomic angles from EXAFS data.[4]

This study of oxygen-bridged iron dimers was initiated in anticipation of the possible influence of intervening atoms in the EXAFS from hemerythrin, an oxygen-transport protein with a dimeric iron active center. In order to make quantitative assessments of the effect of intervening atoms on the Fe–Fe EXAFS scattering, we obtained a series of dimeric iron models of known crystal structure with a variety of bridging geometries. These include dihydroxo- or dialkoxo-bridged dimers and μ-oxo-bridged dimers and trimers. The bridging oxygen atoms in these compounds intervene to varying degrees in the path between the two iron atoms. Our results indicate that where the Fe–O–Fe bridging angle is greater than ca. 150° the intervening oxygen atom in the absorber-to-scatterer path enhances the Fe–Fe EXAFS scattering amplitude and also causes additional phase shifts. The magnitude of the iron EXAFS waves is found to correlate with the Fe–O–Fe bridging angle. Hence, the study of multiple-scattering effects in a series of models of known structure provides an empirical basis for interpreting the results from similar, but unknown, structures.

Experimental Section

Materials. Crystalline samples were acquired for a series of oxygen-bridged iron dimers selected to span a range of bridging angles and hence the degree of possible intervention in the EXAFS scattering. Except where noted, these samples were obtained as gifts directly from the original source for the crystals used in the respective crystallographic structure analyses and were prepared as described in references cited below. The compound analyzed in this study are the following: (I) $[Chel(H_2O)FeOH]_2 \cdot 4H_2O$ (Chel = 4-hydroxy-2,6-pyridinecarboxylate),[5]

(1) (a) Department of Chemistry, Stanford University. (b) Naval Research Laboratory, Washington, D.C.. (c) Department of Applied Physics, Stanford University.

(2) (a) Lee, P. A.; Pendry, J. B. *Phys. Rev. B* **1975**, *11*, 2795–2811. (b) Ashley, C. A.; Doniach, S. *Ibid.* **1975**, *11*, 1279–1288.

(3) Cramer, S. P.; Hodgson, K. O.; Steifel, E. I.; Newton, W. E. *J. Am. Chem. Soc.* **1978**, *100*, 2748–2761.

(4) Teo, B. K. *J. Am. Chem. Soc.* **1981**, *103*, 3990–4001.

(5) Thich, J. A.; Ou, C. C.; Powers, D.; Vasiliou, B.; Mastropaolo, D.; Potenza, J. A.; Schugar, H. J. *J. Am. Chem. Soc.* **1976**, *98*, 1425–1433.

This article not subject to U.S. Copyright. Published 1983 by the American Chemical Society

(II) $[Dipic(H_2O)FeOH]_2$ (Dipic = 2,6-pyridinedicarboxylate),[5] (III) [(SALPA)(SALPAH)Fe]$_2$·toluene (SALPA = dianionic form of (3-hydroxypropyl)salicylaldimine, SALPAH = anionic form),[6] (IV) $[(H_2O)(ala)_2Fe]_3O(ClO_4^-)\cdot 6HClO_4$ (ala = alanine),[7] (V) $K_5[(H_2O)(SO_4)_2Fe]_3O\cdot 7H_2O$,[8] (VI) [(Salen)Fe]$_2$O·$CH_2Cl_2$ (Salen = *N,N'*-ethylenebis(salicylideneamine)),[9] (VII) $[(2\text{-Mequin})_2Fe]_2O$ (2-Mequin = 8-hydroxy-2-methylquinolinato)[10] (VIII) $[(N\text{-}n\text{-propyl-sal})_2Fe]_2O$ (Sal = salicylideneamine),[11] (IX) $enH_2[(HEDTA)Fe]_2O\cdot 6H_2O$ (en = ethylenediamine, HEDTA = *N*-(2-hydroxyethylenediaminetriacetate),[12] (X) $[(N\text{-}p\text{-chlorophenyl-sal})_2Fe]_2O$,[13] (XI) $[Cl\text{-}PDC(H_2O)_2Fe]_2O\cdot 4H_2O$ (Cl-PDC = 4-chloro-2,6-pyridinecarboxylate),[14] (XII) $[HPBT)_2Fe]_2O$ (HPBT = 2-(*o*-hydroxyphenyl)benzothiazole).[15]

The samples of compounds I, II, V, IX, and XI were a gift from Dr. H. J. Schugar of Rutgers University. The samples of compounds VII and XII were a gift from Dr. A. W. Addison of Drexel University. Compound VII was crystallized from 2-methoxyethanol, which is not included in the crystals, rather than from chloroform as in the cited crystal structure report. The three-dimensional structure of compound XII is unknown. The samples of compounds VIII were a gift from Dr. K. S. Murray of Monash University, that of compound III was a gift from Dr. J. A. Bertrand of the Georgia Institute of Technology, and that of compound VI was a gift from Dr. A. T. McPhail of Duke University. Compound IV was prepared by mixing ferric perchlorate with alanine in a 1:2 ratio and evaporating to dryness at room temperature.

Data Collection and Reduction. The EXAFS data were collected by using synchroton radiation at the Stanford Synchrotron Radiation Laboratory. Samples were diluted with Li_2CO_3 and ground to a fine powder which was loaded in an aluminum spacer and sealed with X-ray transparent mylar or Kapton tape. Relative absorption data were measured in transmission mode with ionization detectors. The data were collected using beam line I-5 with a Si[220] monochromator under ring operating conditions of 2.6 GeV and 28 mA maximal current and on beam line II-3 using a Ge[111] monochromator with the ring operated at about 3 GeV and 60 mA average current. At least three scans of about 25 min each were run for each compound out to $\mathbf{k} = 16.5$ Å^{-1}.

Data were processed with procedures described in detail previously[16] and summarized below. Energy was calibrated with respect to an Fe foil by assigning 7111.2 eV to the first inflection point on the absorption edge. A polynomial was fit to the preedge region and subtracted from the whole spectrum of absorption data to isolate the elemental absorption. Then a smooth spline, μ_s, formed from smoothly joined cubic spline segments, was fit to the relative modulation of the isolated Fe absorption coefficient, μ, above the edge. Finally, the photon energy was conveted to photoelectron wave vector $\mathbf{k}$, defined by $\mathbf{k}$ [$[2m(E - E_0)/\hbar^2]^{1/2}$, where m is the mass of electron, E is photon energy, and E_0 the threshold energy of the absorption edge, which is defined to be 7130 eV for Fe K absorption edge. The observed EXAFS spectrum, $\chi(\mathbf{k}) = (\mu - \mu_s)/\mu_0$, was determined by deviations from the smooth spline normalized by the calculated free atom absorption μ_0.

Data Analysis. Interpretation of EXAFS spectra in terms of structural parameters usually depends on the single scattering theory[17] which, for K edge absorption, can be represented as follows:

$$\chi(\mathbf{k}) = \frac{\mu - \mu_s}{\mu_0} = \frac{1}{\mathbf{k}} \sum_s \frac{N_s|f_s(\pi,\mathbf{k})|}{{R_{as}}^2} e^{-\sigma_{as}^2\mathbf{k}^2} e^{-2R_{as}/\lambda} \sin(2\mathbf{k}R_{as} + \alpha_{as}(\mathbf{k})) \quad (1)$$

Each shell, s, has N_s scatterers at a mean distance of R_{as} from the absorbing atoms with a root mean square deviation of σ_{as} in the distance. The electron backscattering amplitudes, $|f_s(\pi,\mathbf{k})|$, and the total phase shifts, α_{as}, depend on scatterer identity. The photoelectron decay factor, $\exp(-2R/\lambda)$, is omitted from this formulation, but its effect is accommodated by parameters in the representation given below. A trial structural model is often deduced by inspection of Fourier transforms of the EXAFS or by reference to the known crystal structure or a hypothetical model.

A least-squares curve-fitting procedure can be effectively used for refinement of a structural model against EXAFS data.[16] In this procedure the EXAFS is modeled by a set of sine waves:

$$\chi(\mathbf{k}) = \sum_s A_s(\mathbf{k}) \sin(\Phi_s(\mathbf{k})) \quad (2)$$

for which the amplitude and phase are parameterized:

$$A_s(\mathbf{k}) = \frac{c_0 e^{-c_1\mathbf{k}^2}}{\mathbf{k}^{c_2}} \quad (3)$$

$$\Phi(\mathbf{k}) = a_0 + a_1\mathbf{k} + a_2\mathbf{k}^2 \quad (4)$$

It is possible to associate certain parameters with particular structure features by identifying the amplitudes and phases of this curve-fitting representation (eq 2–4) with those for the physical theory (eq 1). The set of parameters is obtained empirically from fits to data on compounds of known structure. In a typical unknown structure analysis, a set of parameters for a certain absorber–scatterer pair will be chosen and fit to the EXAFS data, floating only c_0 and a_1 in eq 2–4. Identification of the type of scatterer requires a reasonable fit of the amplitude and the phase. The number of scatterers is determined from c_0. The distance information is readily obtained from a_1 (since the absorber–scatterer distance is $\mathbf{k}$ dependent).

Fourier filtering is used to isolate and analyze the EXAFS contribution from a particular shell of scatterers. This is done by Fourier transforming the EXAFS data (usually weighted by $\mathbf{k}^3$) over a broad range of $\mathbf{k}$ values, filtering this transform through a window of distances about a peak of interest, and then back-transforming into $\mathbf{k}$ space. The filtered EXAFS spectrum for the isolated component is then fitted by the least-squares procedure described above. Our approach in the present study has been to analyze the Fe–Fe scattering waves for the various compounds in terms of the single scattering procedures outlined above.

Results and Discussion

The series of oxygen-bridged iron dimer model compounds we selected for this study included two dihydroxo- and dialkoxo-bridged dimers, two μ-oxo-bridged trimers, and seven μ-oxo-bridged dimers, with the range of Fe–O–Fe bridging angles spanning 103°–180°. For the sake of consistency and convenience, we have adopted a schematic representation ABC used by Teo[4] to illustrate the Fe–O–Fe system, with A as the absorbing Fe atom, B as the bridging oxygen atom, and C as the scattering Fe atom. There are three major paths in the ABC system by which an electron can propagate out and back from an absorber at A to the scatterer at C: (I) A–C–A, the direct pathway assumed in the single-scattering theory, (II) A–B–C–A or A–C–B–A, the triangular indirect pathway involving the intervening atom on only one of the trips, and (III) A–B–C–B–A, the indirect pathway involving the intervening atom on both trips. Naturally, for the compounds with the iron atoms bridged by two oxygen atoms, pathways II and III should be treated twice. Herein we define the path lengths traveled for these major pathways by

$$r_I = r_{AC}$$

$$r_{II} = \frac{r_{AB} + r_{BC} + r_{AC}}{2}$$

$$r_{III} = r_{AB} + r_{BC} \quad (5)$$

Simple calculations show that the three path lengths do not differ significantly when the A–B–C bridging angle is large. For example, assuming an average Fe–O distance of 1.90 Å (i.e., $r_{AB} = r_{BC} = 1.90$ Å), then r_I, r_{II} and r_{III} are 3.79, 3.79, and 3.80 Å when the bridging angle is 170°, and 3.67, 3.74, and 3.80 Å when the bridging angle is 150°. Even at the smaller bridging angle, the difference of path lengths is not sufficient for the scattering peaks to be resolved in the Fourier transform. Under such circumstances, the Fe–Fe EXAFS peak would be observed as a single

(6) Bertrand, J. A.; Eller, P. G. *Inorg. Chem.* **1974**, *13*, 927–934.
(7) Holt, E. M.; Holt; S. L.; Tucker, W. F.; Asplund, R. O.; Watson, K. J. *J. Am. Chem. Soc.* **1974**, *96*, 2621–2623.
(8) (a) Giacovazzo, C.; Scordari, F.; Menchetti, S. *Acta Crystallogr., Sect. B* **1975**, *B31*, 2171–2173. (b) Schugar, H., unpublished results.
(9) Coggon, P.; McPhail, A. T.; Gross, P. N.; Mabbs, F. E.; McLachlan, V. N. *J. Chem. Soc. A* **1971**, 1014–1019.
(10) Mabbs, F. E.; McLachlan, V. N.; McFadden, D.; McPhail, A. T.; Gross, P. N. *J. Chem. Soc., Dalton Trans.* **1973**, 2016–2024.
(11) Davies, J. E.; Gatehouse, B. M. *Cryst. Struct. Commun.* **1972**, *1*, 115–120.
(12) Lippard, S. J.; Schugar, H.; Walling, C. *Inorg. Chem.* **1967**, *6*, 1825–1831.
(13) Davies, J. E; Gatehouse, B. M. *Acta Crystallogr., Sect. B* **1973**, *B29*, 2651–2658.
(14) Ou, C. C.; Wollmann, R. G.; Hendrickson, D. N.; Potenza, J. A.; Schugar, H. J. *J. Am. Chem. Soc.* **1978**, *100*, 4717–4724.
(15) Prepared by A. W. Addison, Diffraction-quality crystals have not been obtained.
(16) Cramer, S. P.; Hodgson, K. O. *Prog. Inorg. Chem.* **1979**, *15*, 1–39.
(17) (a) Sayers, D. E.; Lytle, F. W.; Stern, E. A. *Adv. in X-Ray Anal.* **1970**, *13*, 248–271. (b) Sayers, D. E.; Stern, E. A.; Lytle, F. W. *Phys. Rev. Lett.* **1971**, *27*, 1204–1207.

peak in the Fourier transform. However, the situation would be different when the A–B–C bridging angle is small. For example, still assuming $r_{AB} = r_{BC} = 1.90$ Å, the three corresponding path lengths would then be 3.29, 3.55, and 3.80 Å when the bridging angle is 120°, and 2.91, 3.36, and 3.80 Å when the bridging angle is 100°. In these cases, it is expected that one would observe resolved peaks in the Fourier transform for the three different scattering pathways. In the following sections, we examine the series of Fe–O–Fe compounds and investigate the effect of the bridging oxygen atom on the analysis of iron backscattering EXAFS waves.

One of the most difficult parts in the analysis of outer-shell backscatters is the isolation of a resolved peak for curve fitting. Under most circumstances, second-shell atoms from the ligating groups will be present with a range of distribution of distances from the absorbing atom. Furthermore, since these atoms are not directly coordinated to the central atom, their relative motion with respect to the central atom will often be somewhat uncorrelated, giving rise to undetermined Debye–Waller factors. Thus, the identification of atom type and estimation of number of backscatterers for backscatterers beyond the first shell is more difficult. Since these second-shell ligand atoms will be mostly low Z atoms, it will be difficult to identify a specific low Z atom of interest from the matrix of low Z ligand atoms. Fortunately, high Z atoms, possessing different backscattering amplitude envelope of higher amplitude and a different phase shift, offer the possibility of distinguishing the high Z backscatterer from the matrix of low Z backscatterers. Such a possibility would be enhanced by extending the data collection to higher **k** space, considering that (i) backscattering amplitude maxima generally move to higher **k** as Z increases, and (ii) the backscattering from nonbonding outer-shell ligand atoms, having a large Debye–Waller factor, dies out much faster at high **k**. Collecting the data to higher **k** space also offers better resolution in Fourier transform space.

EXAFS of [(Chel)(H$_2$O)FeOH]$_2$ and Related Compounds. [(Chel)(H$_2$O)FeOH]$_2$ is chosen for a detailed discussion as a representative of an Fe–O–Fe system with a small bridging angle. The compound offers a unique situation since the only outer-shell ligand atoms present within a 4-Å radius of the central absorbing iron atom are several carbon atoms from 2.90 to 2.95 Å from the absorbing atom and the bridged iron atom. This presents an excellent opportunity for the iron backscatterer, which is 3.08 Å from the absorbing atom, to be resolved. A one-dimensional radial distribution function[18] from the absorbing atom, calculated from published crystal structure, is given in Figure 1a. The first peak at 2 Å represents the first coordinated shell of nitrogen and oxygen atoms. The second peak represents the shell of carbon atoms and the third peak (shaded) an iron backscatterer.

The EXAFS spectrum for [(Chel)(H$_2$O)FeOH]$_2$ is given is Figure 2a. This spectrum has been shown to be reproducible and represents an spectrum of superb quality which is not likely to be attainable for systems of low metal concentration. The overall amplitude envelope decays rapidly at high **k**. Irregularities on the sine curve and particularly a beat at **k** = 13 Å^{-1} indicate the presence of more than one shell. A Fourier transform over a **k** range of 4–12 Å^{-1} is given in Figure 1b. This is the usual working range for most published work.[19] A transform over a larger **k** range of 4–16 Å^{-1} is also given in Figure 1c. In this transform, much better resolution of outer shell peaks is obtained. It will be desirable to compare this transform to Figure 1a, obtained by calculation from crystallographic results. As usual, it should be noted that about 0.2–0.5 Å should be added to peak positions in the transform to obtain the real distance because of a distance shift not taken into account in the Fourier transformation. The value of the distance shift is somewhat variable and depends on the absorber–scatterer type. However, the major peak in Figure 1c can be nicely correlated to the first peak in Figure 1a, after adding 0.3 Å distance shift. The small peaks on both sides of the main peak can be attributed to truncation and nonlinearity effects in the Fourier transformation. The first outer shell peak at 2.6 Å in Figure 1c can then be related to the second peak in Figure 1a which is a shell of carbon atoms. Indeed, Fourier filtering and curve-fitting analysis shows a shell of carbon atoms at 2.95 Å, consistent with crystallographic results.

An interesting result is observed comparing the third peak (at highest R) in Figure 1a to the corresponding peak in Figure 1c. Instead of only the one peak expected, three peaks (the third one partly resolved from the second) occurring at 2.9, 3.2, and 3.5 Å in the transform are observed. This is at first puzzling, until one considers the multiple scattering pathways possible with the backscattering iron. Adopting the nomenclature defined earlier,

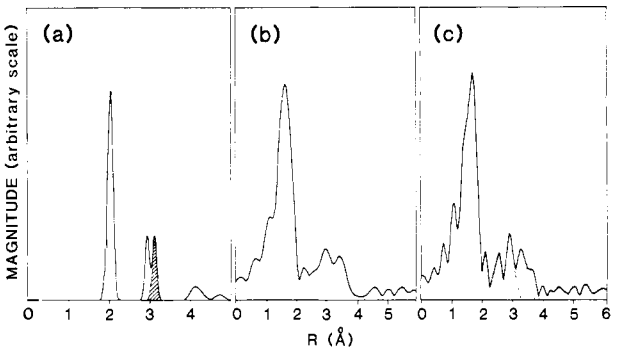

Figure 1. [(Chel)(H$_2$O)FeOH]$_2$: (a) One-dimensional radial distribution function calculated from crystallographic results. The shaded peak represents the iron backscatterer. (b) Fourier transform of EXAFS taken over a **k** range of 4–12 Å^{-1}, **k**^{3} weighted. (c) Fourier transform of EXAFS taken over a **k** range of 4–16 Å^{-1}, **k**^{3} weighted. The magnitude of the peak height is relative (see text). The peaks assigned to the three scattering pathways are resolved in dotted lines in (c).

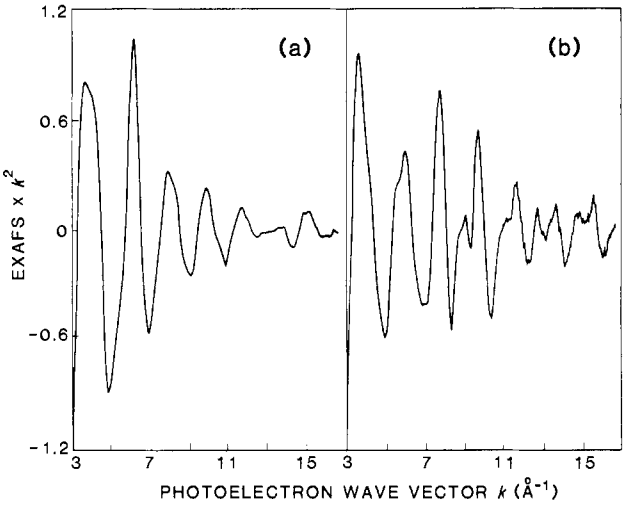

Figure 2. EXAFS spectra of (a) [(Chel)(H$_2$O)FeOH]$_2$ and (b) [(Cl-PDC)(H$_2$O)$_2$Fe]$_2$O. EXAFS is multiplied by **k**^{2}.

(18) The one-dimensional radial distribution function about the central atom is synthesized from the interatomic distances calculated from the crystal structure, according to the following expression:

$$P(R) = \sum_i \frac{A_i}{\sigma_i R_i^{02}} e^{-\gamma R_i^0} e^{-(R-R_i^0)^2/2\sigma_i^2}$$

where

$$A_i = 1/N_{Fe},\ X = C, N, O$$
$$4/N_{Fe},\ X = Fe$$

$$\sigma_i = 0.05\ Å,\ R^0 \le 3.0\ Å$$
$$0.10\ Å,\ R^0 \ge 3.0\ Å$$

(19) (a) Cramer, S. P.; Dawson, J. H.; Hodgson, K. O.; Hager, L. P. *J. Am. Chem. Soc.* **1978**, *100*, 7282–7290. (b) Eigenberger, P.; Shulman, R. G.; Kincaid, B. M.; Brown, G. S.; Ogawa, S. *Nature (London)* **1978**, *274*, 30–34. (c) Shulman, R. G.; Eisenberger, P.; Blumberg, W. E.; Stombaugh, N. A. *Proc. Natl. Acad. Sci. U.S.A.* **1975**, *72*, 4003–4007.

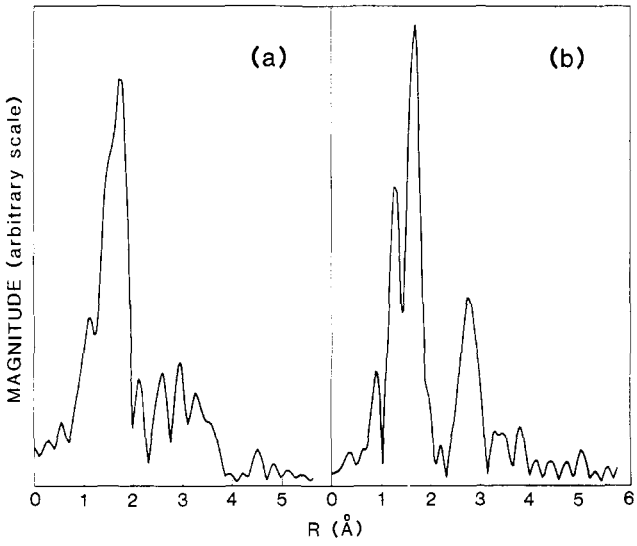

Figure 3. Fourier transform of EXAFS for (a) $[(Dipic)(H_2O)FeOH]_2$, and (b) $[(H_2O)(Ala)_2Fe]_3O$, both taken over a **k** range of 4–16 Å^{-1}, **k**^{3} weighted.

we have r_{AB} = 1.94 Å, r_{BC} = 1.99 Å, that calculates r_I = 3.08 Å, r_{II} = 3.51 Å, and r_{III} = 3.93 Å for an A–B–C angle of 103°. Correlating the transform peaks to the path lengths suggests linear phase shifts of ca. 0.2, 0.3, and 0.4 Å in the transform. The first phase shift of 0.2 Å toward low R can be reasonably attributed to the linear distance shift inherent in Fourier transformation. The additional shift of 0.1 and 0.2 Å toward lower R values in the pathways II and III is attributed to the effects of scattering by the intervening oxygen atom(s) as the photoelectron travels rom the absorber to the scatterer and back, diffracted by the intervening oxygen atom(s) once and twice, respectively. This is the first evidence that multiple-scattering pathways are observed and identified in a transform (see Figure 1c). Each peak was independently Fourier filtered and back-transformed into the **k** space for curve-fitting analysis to obtain a quantitative measurement of interatomic distances. The best fit of the phases (using the parameters derived from the pathway III of $[(Chel\text{-}PDC)(H_2O)_2Fe]_2O$) calculates 3.08, 3.40, and 3.71 Å for the three filtered waves. This indicates that a linear phase shift of −0.11 Å is encountered as the photoelectron is scattered by the intervening oxygen atom once, thereby causing a prediction of 0.11-Å shortfall in the calculation of distances for pathway II and a 0.22-Å shortfall for pathway III.

It is also interesting to note that, in the curve-fitting analysis of the backscattering peak via pathway II, an introduction of approximately π to the constant term of the parameterized phase shift is essential to generate a reasonable fit. This additional phase shift is consistent with Teo's calculation using a multiple-scattering formalism.[4] The additional factor in phase shift can be explained as the time delay effect when the photoelectron propagates through the potential of the oxygen atom. Such correction becomes unnecessary in the curve-fitting analysis of the backscattering peak via pathway III, since another π will be introduced into the constant term of the phase shift as the photoelectron propagates through the potential of the oxygen atom one more time in this pathway.

Another dimeric iron model $[(Dipic)(H_2O)FeOH]_2$ with an Fe–O–Fe angle of 104° was also examined. A Fourier transform for this compound is given in Figure 3a. A similar interpretation is applicable to this compound. Almost identical results were obtained for this compound as for $[(Chel)(H_2O)FeOH]_2$. We also collected data on a dialkoxo-bridged dimer $[(SALPA)(SALPAH)Fe]_2$ and two μ-oxo-bridged trimers, $[(H_2O)(SO_4)_2Fe]_3O$ and $[(H_2O)(ala)_2Fe]_3O$. However, interpretation of data for these three compounds becomes more complex as the outer shell ligand atoms are present within unresolvable distances of the iron backscatterer. The transform for $[(H_2O)(ala)_2Fe]_3O$ is given in Figure 3b as an example. The outer shell peak is comprised of four carbon atoms around 3 Å, four oxygen atoms from 3.2–3.4 Å, and two iron atoms at 3.3 Å. Such circumstances make analysis quite difficult.

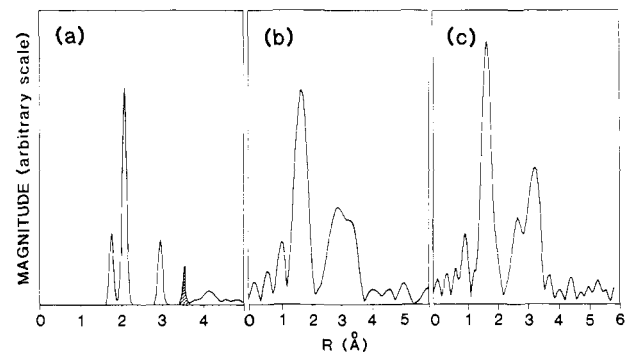

Figure 4. $[(Cl\text{-}PDC)(H_2O)_2Fe]_2O$: (a) One-dimensional radial distribution function calculated from crystallographic results. The shaded peak represents the iron backscatterer. (b) Fourier transform of EXAFS taken over a **k** range of 4–12 Å^{-1}, **k**^{3} weighted. (c) Fourier transform of EXAFS taken over a **k** range of 4–16 Å^{-1}, **k**^{3} weighted. Enhancement in the backscattering peak at 3 Å is prominent in the transform over a larger **k** range. The Fourier-filtered wave of this peak is given in Figure 5a.

EXAFS of $[(Cl\text{-}PDC)(H_2O)_2Fe]_2O$. The calculations described earlier show that the differences in path lengths I, II, and III become very small when the A–B–C bridging angle approaches linearity. For example, even for a 30° deviation from linearity, i.e., for A–B–C angle of 150° and with the assumption of typical Fe–O distances in μ-oxo-bridged dimers (i.e., $r_{AB} = r_{BC}$ = 1.80 Å), the three respective path lengths will be 3.48, 3.54, and 3.60 Å. Such close-lying backscattering peaks will not be easily resolved and will appear as a single broadened peak in a Fourier transform. Furthermore, when the atoms are arranged in an approximately collinear array, the outgoing as well as the incoming photoelectron will be strongly forward scattered by the intervening atom, resulting in a significant amplitude enhancement of multiple-scattering waves. The intervening atom will also cause a phase shift as the photoelectron propagates through the potential of the intervening atom. Such effects are demonstrated by a series of μ-oxo bridging dimeric iron compounds with the oxygen atoms acting as the intervening atom. Since forward scattering is strongly angular dependent,[2a] varying the Fe–O–Fe bridging angle should result in angular dependence in the amplitude of iron backscatterer. The EXAFS spectrum for $[(Cl\text{-}PDC)(H_2O)_2Fe]_2O$ is given in Figure 2b. This compound is selected for discussion owing to the simplicity of the radial distribution of outer shell atoms. A one-dimensional radial distribution function from the absorbing iron atom calculated from published crystal structure[14] is given in Figure 4a. The iron backscattering peak is found at 3.55 Å from the central atom and is well separated from a shell of carbon atoms which is found at about 3.0 Å from the central atom. The other ligand atoms are found at longer distances, ca. 4 Å from the central atom. The Fourier transform of EXAFS data over the range of **k** = 4–12 Å^{-1} is shown in Figure 4b and that from the range of **k** = 4–16 Å^{-1} is shown in Figue 4c. The positions of major peaks in these transforms correspond well with distances from the crystal structure. The first major peak at 1.7 Å is assigned to the first coordination shell of oxygen and nitrogen backscatterers. The small peak at 1.1 Å is not real but an artifact caused by the residual background and transformation of nonlinear phase shifts. The next prominent peaks are assigned to carbon atoms of the ligand and the bridged iron atom. These two shells are poorly resolved in the short-range transform, but inclusion of data to **k** = 16 Å^{-1} not only provides better resolution into peaks at 2.7 and 3.2 Å but also greatly enhances the outer peak. This enhancement suggests that the 3.2-Å peak is due to the iron backscatterer. A comparison of theoretical backscattering amplitudes[20] for carbon and iron shows that, while both have similar

(20) Teo, B. K.; Lee, P. A. *J. Am. Chem. Soc.* **1979**, *101*, 2815–2832.

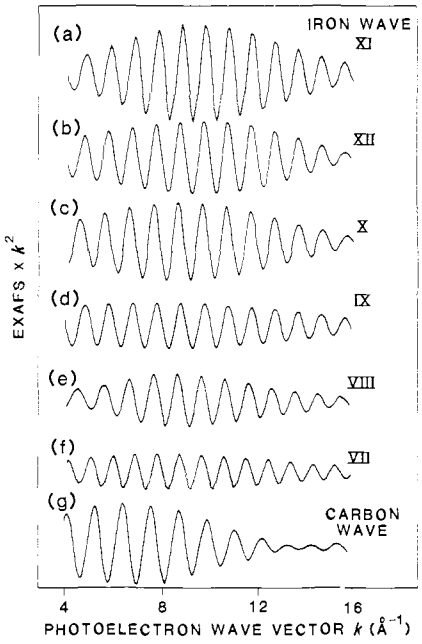

Figure 5. Fourier-filtered Fe waves derived from (a) $[(Cl\text{-}PDC)(H_2O)_2Fe]_2O$, (b) $[(HPBT)_2Fe]_2O$, (c) $[(Cl\text{-phenyl-sal})_2Fe]_2O$, (d) $enH_2[(HEDTA)Fe]_2O$, (e) $[(N\text{-}n\text{-propyl-sal})_2Fe]_2O$, (f) $[(2\text{-Mequin})_2Fe]_2O$, and (g) Fourier-filtered carbon wave derived from $[(Cl\text{-}PDC)(H_2O)_2Fe]_2O$. Note that the carbon wave peaks at lower **k** and damps out much faster at higher **k**.

scattering power at low **k** (e.g., 0.36 for C and 0.43 for Fe at $\mathbf{k} = 4$ Å^{-1}), iron is a much stronger scatterer at high **k** (0.25 for Fe compared to 0.03 for C at $\mathbf{k} = 13$ Å^{-1}). In fact, as we quantify below, the height of this peak also reflects a large amplification due to the intervening atom effect.

The isolated EXAFS wave from the iron backscattering in $[(Cl\text{-}PDC)(H_2O)_2Fe]_2O$ was obtained by back-transforming the iron peak through a Fourier filter of 2.80–3.60 Å and is shown in Figure 5a. For comparison, the filtered EXAFS of the 2.7 Å from the transform is shown in Figure 5g. The amplitude envelope of these filtered EXAFS waves are characteristic of high Z and low Z backscatterers, respectively, and corroborate the assignment to Fe and C in these cases. The Fe–Fe wave was fitted, with $\mathbf{k}^3$ weighting, by the functional form of eq 2 to give the least-squares value of all six parameters. The phase parameters were defined by fitting to the well-defined Fe scattering peak from the direct pathway I in $[(Chel)(H_2O)FeOH]_2$ which has an Fe–Fe separation of 3.08 Å. The phase value calculates the Fe–Fe separation to be 3.34 Å for $[(Cl\text{-}PDC)(H_2O)_2Fe]_2O$. This distance is 0.21 Å shorter than the value of 3.55 Å expected from the crystallographic result. However, we find that in practice pathway III dominates in this linear Fe–O–Fe system. This EXAFS wave can be attributed to the indirect pathway III, by which the photoelectron is scattered by the intervening oxygen atom twice, once on its way from the absorber to the scatterer and once on its way back. We have previously determined that a phase shift of –0.11 Å is encountered when the photoelectron is scattered by an oxygen atom. The calculation of 0.21-Å shortfall for the separation of Fe–Fe in $[(Cl\text{-}PDC)(H_2O)_2Fe]_2O$ is consistent with what is expected with the multiple-scattering pathway III.

Angle Determination by EXAFS. Angle determination by EXAFS has been claimed to be possible via a multiple-scattering formalism by Teo, to an accuracy of better than ca. 5°.[4] This study has shown that such a claim is perhaps overly optimistic. Recently, Boland et al.[21] has criticized Teo's multiple-scattering theory as incomplete. Our studies indicate that angle determination by EXAFS is possible only when outer-shell peaks are well resolved and can be correctly identified. Such cases are infrequent, however, especially for an unknown system. The chance of correctly identifying an outer-shell peak will be enhanced when the interested backscatterer is distinguishable from other atoms, e.g., distinguishing a high Z atom from a matrix of low Z atoms (since high Z scatterers generally have backscattering amplitude envelope maxima at higher **k**).

(21) Boland, J. J.; Crane, S. E.; Baldeschwieler, J. D. *J. Chem. Phys.* **1982**, *77*, 142–153.

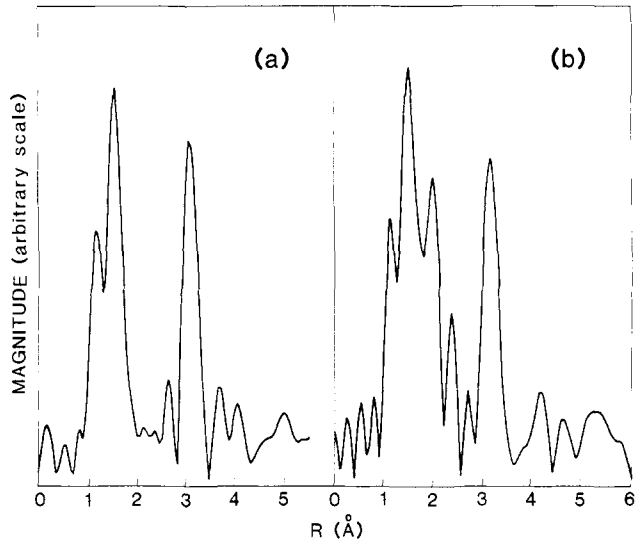

Figure 6. Fourier transforms of EXAFS for (a) $[(Cl\text{-phenyl-sal})_2Fe]O$, and (b) $[(HPBT)_2Fe]$, both taken over a **k** range of 4–16 Å^{-1}, with $\mathbf{k}^3$ weighting. The magnitude of the peaks is relative (see text). Fourier-filtered waves of the 3-Å peaks are given in Figure 5c and 5b, respectively.

This study with a series of μ-oxo bridging dimeric iron compounds shows that it is possible to estimate the Fe–O–Fe bridging angle by an EXAFS analysis of backscattering iron when the bridging angle is larger than ca. 150°. The series of compounds includes $[(Cl\text{-}PDC)(H_2O)_2Fe]_2O$, $[(Cl\text{-phenyl-sal})_2Fe]_2O$, $enH_2[(HEDTA)Fe]_2O$, $[(N\text{-}n\text{-propyl-sal})_2Fe]_2O$ and $[(2\text{-Mequin})_2Fe]_2O$ with respective Fe–O–Fe bridging angles of 180°, 175°, 165°, 164°, and 152° and $[(HPBT)_2Fe]_2O$ whose crystallographic structure is not known. The Fourier transform of $[(Salen)Fe]_2O\cdot CH_2Cl_2$ with a Fe–O–Fe bridging angle of 142° gave a complicated spectrum from which we were unable to isolate an Fe–Fe backscattering peak and no further analysis was pursued for this compound. A typical transform of the EXAFS data over a **k** range of 4–16 Å^{-1} is shown in Figure 6a for $[(Cl\text{-phenyl-sal})_2Fe]_2O$. It will at once be noticed that a prominent peak is observed at 3.1 Å in the transform. The peak is typical of all compounds of similar structures. It might be argued that at least three peaks should be observed for the multiple-scattering pathways as was observed in $[(Chel)(H_2O)FeOH]_2$. The three path lengths that give rise to the resolved peaks for $[(Chel)(H_2O)FeOH]_2$ are very close when the bridging angle is large; indeed, all fall within 0.2 Å which is usually not resolvable in a transform over this range. Futhurmore, the EXAFS amplitude enhancement will be much more prominent for pathway III than pathways II and I when the Fe–O–Fe system is close to linearity because of the strong forward scattering effect.[2a] This assertion was indeed confirmed by Teo's calculations using a multiple-scattering formalism.[4] This backscattering peak can then be interpreted as an Fe backscattering peak mainly due to the multiple-scattering pathway III with minor contribution from the other pathways. The outer-shell low Z ligand atoms will not be expected to contribute significantly compared to iron backscattering because of the lower scattering power of low Z atoms and also because of the atomic arrangement that always leads to large static disorder causing destrucvtive interference among themselves. However, when the outer-shell ligand atoms are arranged in a way such that destructive interference is not significant, outer-shell peaks for the ligand atoms should be observed, as is the case of $[Cl\text{-}PDC(H_2O)_2Fe]_2O$ (Figure 4c).

The Fourier filtering technique was applied to filter out the backscattering peaks for all compounds; the filtered EXAFS are

Table I. EXAFS Analysis of the Iron Backscattering Wave as a Function of Fe–O–Fe Bridging Angle

compd	Fe-O-Fe, deg	EXAFS resuls: function value[a]	EXAFS resuls: magnitude[b] (arb scale)	EXAFS resuls: obsd distance,[c] Å	Fe–Fe distance: calcd from EXAFS[d]	Fe–Fe distance: detmd from exptl
$[(Cl\text{-}PDC)(H_2O)_2Fe]_2O$	180	0.10	4.0	3.34	3.56	3.55
$[(Cl\text{-}phenyl\text{-}sal)_2Fe]_2O$	175	0.46	2.8	3.34	3.56	3.53
$enH_2[(HEDTA)Fe]_2O$	165	0.13	2.0	3.34	3.53	3.56
$[(N\text{-}n\text{-}propyl\text{-}sal)_2Fe]_2O$	164	0.16	1.9	3.36	3.54	3.51
$[(2\text{-}Mequin)_2Fe]_2O$	152	0.20	1.5	3.35	3.46	3.45
$[(HPBT)_2Fe]_2O$	*e*	0.19	3.1	3.34	3.56	*e*

[a] Fits are done by minimizing the difference between the observed and calculated EXAFS at each point in k space, squared, and then weighted by k^6. The minimization function value F is given by $F^2 = \Sigma[k^6(\text{data} - \text{fit})^2]/N$. [b] The magnitude is arbitrarily scaled to be unity for magnitude of EXAFS wave obtained from the direct pathway I for compound I, i.e., a compound of small bridging angle. [c] These distances are calculated with respect to phase shifts which were extracted from compound XI and calibrated with respect to the direct pathway I from compound I. [d] A phase shift of 0.22 Å is added to the distances obtained from curve-fitting analysis to reflect the phase shift caused by the photoelectron twice entering the potential of the intervening oxygen atom. Fe-Fe distance is calculated based on the knowledge of the lengths of two sides of an isosceles triangle and the included angle. [e] The X-ray crystallographic structure for this compound is not available. EXAFS analysis predicts a Fe-O-Fe bridging angle of 177° and a Fe-Fe separation of 3.56 Å.

given in Figure 5a–f. It is interesting to note that they all have similar amplitude envelopes. Compared to Figure 5a where the Fe–O–Fe atoms are arranged in a linear array and the dominant pathway is via pathway III, this is consistent with our previous assertion that the peaks in these transforms are mainly due to scattering via the multiple-scattering pathway III. The amplitude of the filtered EXAFS for $[(Mequin)_2Fe]_2O$ is the smallest of all. This can be explained by the diminished contribution by scattering via the pathway III because of the decreased bridging angle (152°), i.e., reduced forward scattering as a result of increased scattering angle.

Quantitative comparison of the filtered EXAFS were performed by a nonlinear least-squares curve-fitting analysis. Fe–Fe parameters were obtained by fitting, with $\mathbf{k}^3$ weighting, with the functional form of eq 2 to the iron backscattering peak of $[Cl\text{-}PDC(H_2O)_2Fe]_2O$. The phase parameters were calibrated so as to give 3.08 Å when they were transferred to fit the well-defined backscattering wave denoted by the pathway I for $[(Chel)(H_2O)FeOH]_2$. The values of magnitude reported here are relative, defined to calculate one atom for the backscattering wave given by $[(Chel)(H_2O)FeOH]_2$.

The Fe–Fe pairwise parameters are then transferred to the filtered EXAFS, floating c_0 and a_1 for an optimal fit. All fits were indeed very good, giving small function values.[22] A two-wave fit including a shell of carbon atoms often improves the function value of the fits but usually does not change the EXAFS results significantly. Curve-fitting results are summarized in Table I. It is interesting to note that the magnitude obtained from the curve-fitting analysis is strongly correlated to the Fe–O–Fe bridging angle, with maximum enhancement found when Fe–O–Fe is linear. The magnitude drops sharply with a deviation from linearity, and the falloff rate slows down as the Fe–O–Fe angle is further reduced, as shown in Figure 7. This correlation between the magnitude of EXAFS waves and the bridging angles can provide an empirical basis for angle determination by EXAFS for the series of homologous iron complexes. The backscattering peak is Fourier filtered and curve fit to determine an unknown bridging angle of similar structure. The magnitude given by the optimal fit should reflect the bridging angle. We have collected data on a μ-oxo-bridged dimeric compound $[(HPBT)_2Fe]O$, for which the crystallographic structure is not yet solved. The EXAFS analysis calculates a magnitude of 3.1 which is indicative of a bridging angle of ca. 177°. The solution of the structure of this compound will be an unbiased check of the technique for angle determination. We have also applied this technique to determine the bridging angle for a μ-oxo-bridged dimeric iron protein, hemerythrin, and calculate the bridging angle to be ca. 165°.[23]

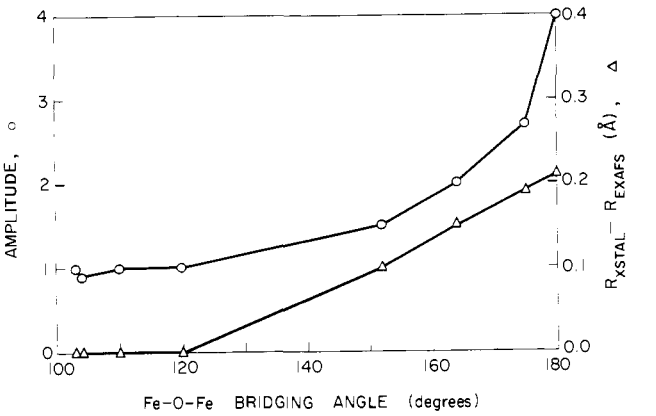

Figure 7. Plot of the amplitude of the Fe EXAFS waves vs. the Fe–O–Fe bridging angles in a series of oxygen-bridged dimeric iron compounds. Note that the amplitude enhancement is a function of bridging angle. The bridging angle of unknown compounds with similar structure can be determined from the curve. The curve in triangles gives the difference in distances as determined from crystallographic studies and from EXAFS (without phase correction), i.e., difference of distances in columns 5 and 7 in Table I.

Fe–Fe Distance Determination. This technique also allows determination of the Fe–Fe interatomic distances. When the bridging angle is small, the Fe–Fe distance can be determined directly from pathway I, if the direct scattering peak can be readily resolved from other scatterers. However, when the bridging angle is large, scattering via direct pathway I cannot be resolved and its magnitude will be relatively small compared to the multiple-scattering pathway III, making direct measurement of Fe–Fe distance impossible. Nevertheless, given the path lengths of pathway III and the bridging angle, it is possible to calculate the interatomic Fe–Fe distance in the following manner. A linear phase shift of 0.22 Å is added to the distance obtained from curve-fitting analysis to reflect the phase shifts caused by the photoelectron scattered by the bridging oxygen atom twice, once on its way to the scatterer and once on its way back to the absorber. The Fe, O, and Fe atoms can be approximated to form an isosceles triangle. Knowing two of the sides and an angle allows us to calculate the other side, which is the Fe–Fe distance we wish to know. Such procedures were applied to the series of compounds we examined and the agreement was found to be reasonable, predicting distances to within ±0.05 Å of the crystallographically determined distances. Such agreement shows that our peak assignment and subsequent analysis were correct and the application of the technique for angle determination and interatomic distance calculation for a partially known system is possible.

Naturally, one would expect the phase shift for pathway III to be dependent on the scattering angle. Our empirical approach with the models, however, indicates that the phase shifts are transferable among models of different bridging angles in the range

(22) Fits are done by minimizing the difference between the observed and calculated EXAFS at each point in **k** space, squared, and then weighted, by $\mathbf{k}^6$. The minimization function value F is given by $F^2 = \Sigma[\mathbf{k}^6(\text{data} - \text{fit})^2]/N$.

(23) Hendrickson, W. A.; Co, M. S.; Smith, J. L.; Hodgson, K. O.; Klippenstein, G. L. *Proc. Natl. Acad. Sci.* U.S.A. **1982**, *79*, 6255–6259.

of 150° and 180°. This is, in fact, consistent with Teo's calculations showing that the scattering phases are quite similar between the scattering angles of 0° and 30° (bridging angles of 180° and 150°), despite the enormous variation of scattering amplitudes. The insensitivity of phase shifts as a function of scattering angles thus allows us to transfer the parameterized phase shifts for distance determination.

Conclusion

In this paper, we have examined the X-ray absorption spectra of a series of oxygen-bridged iron complexes and demonstrated the effect of the intervening oxygen atom on the analysis of outer-shell iron waves. The results indicated that for compounds of Fe–O–Fe bridging angle ca. 100°, the three scattering pathways are resolvable and can be analyzed independently to find the Fe–Fe distance. When the bridging angle increases, the multiple-scattering pathways become dominant. The multiple-scattering pathway III is signified by an enhancement in amplitude which is directly related to the bridging angle of the system. The largest enhancement is found in the linear Fe–O–Fe system, of which the amplitude of the scattered iron wave is magnified by a factor of 4. The phase is also found to be shifted by approximately π in the constant part and about −0.1 Å in the linear part as the photoelectron propagates through the potential of the oxygen atom with a scattering angle of 103°. The variation of the phase as a function of scattering angle in the range of 0° and 30° is found to be small, not significant in the analysis.

The analysis of the series of compounds has shown that for an isolated backscattering peak, it is possible to estimate the bridging angle to ±8° and calculate the metal–metal distance to within ±0.05 Å. This method has been applied to examine a dimeric iron system in hemerythrin and calculates an Fe–O–Fe angle of 165° and an iron–iron distance of 3.38 Å. The work also illustrates that care must be exercised in interpreting EXAFS of neighboring atoms beyond the first coordination shell.

Acknowledgment. We thank Dr. H. J. Schugar, Dr. A. W. Addison, Dr. K. S. Murray, Dr. J. A. Bertrand, and Dr. A. T. McPhail for donation of compounds for this study. We also thank Dr. Robert A. Scott, Dr. Janet L. Smith, Jim Hahn, and Steve Conradson for helpful discussions. This work was supported in part by the National Science Foundation through Grant PCM-79-04915. Synchrotron radiation time for the EXAFS work was provided by the Stanford Synchrotron Radiation Laboratory, supported by the National Science Foundation (DMR 77-27489) and the National Institutes of Health (RR-01209).

Registry No. I, 58982-68-6; II, 58982-69-7; III, 49788-37-6; IV, 55134-47-9; V, 56968-10-6; VI, 19633-03-5; VII, 51331-59-0; VIII, 20559-32-4; IX, 18024-73-2; X, 19555-43-2; XI, 67477-28-5; XII, 84237-93-4.

Molybdenum Chalcogenides: Clusters, Chains, and Extended Solids. The Approach to Bonding in Three Dimensions

Timothy Hughbanks and Roald Hoffmann*

Contribution from the Department of Chemistry and Materials Science Center, Cornell University, Ithaca, New York 14853. *Received July 29, 1982*

Abstract: A combined molecular orbital and crystal orbital analysis of systems containing $Mo_{3n}X_{3n+2}$ (n = 2, 3, 4, ∞; X = S, Se, Te) units is presented. The modes of packing Mo_6X_8, Mo_9X_{11}, and $Mo_{12}X_{14}$ clusters into crystals are explained in terms of the cluster frontier orbitals. Intercluster Mo–X bonds are seen to result from an interaction between chalcogen donor orbitals and the cluster LUMO's that are localized on Mo atoms residing in the "square faces" of the clusters. Closed-shell electron counts for the clusters are elucidated. The relationship between the cluster frontier orbitals and surface states is discussed. Finally, relationships between the band structure of $(Mo_3X_3^-)_\infty$ chains and the finite cluster molecular orbitals are explained.

Structural Overview

For over a decade, compounds known as the "Chevrel phases"[1] have excited solid-state chemists and physicists. The prime reason for sustained interest in these compounds has undoubtedly lain in their conducting properties; these ternary molybdenum chalcogenide materials include both high-temperature and very high-field superconductors.[2] Most of these materials can be described by the formula MMo_6X_8, where M = Pb, Sn, Ba, Au, Cu, Li, etc. and X is usually S, Se, or Te (though compounds containing halogens have been prepared). Compounds in which some Mo atoms are replaced by Re, Ru, and Rh have also been made.[3,4]

The fundamental structural unit to be found in the Chevrel phases is the cluster Mo_6X_8 displayed in three different and geometrically pleasing ways in **1**. In **1a** an octahedron of molybdenums (Mo–Mo ≅ 2.7 Å) is encased in a cube of chalcogens (Mo–S ≅ 2.45 Å or Mo–Se ≅ 2.6 Å). **1b** exhibits the same cluster as consisting of an octahedron with its triangular faces capped by chalcogenides; this view emphasizes the connectivity within the cluster. In **1c** the cluster has been reoriented so that a 3-fold

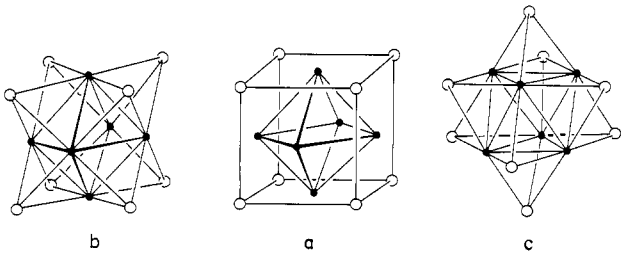

1

(1) Chevrel, R.; Sergent, M.; Prigent, J. *J. Solid State Chem.* **1971**, *3*, 515–519.
(2) For reviews, see: (a) Fisher, Ø. *Appl. Phys.* **1978**, *16*, 1–28. (b) Chevrel, R. In "Superconductor Materials Science: Metallurgy, Fabrication and Applications"; Foner, S., Schwartz, B. B., Eds.; Plenum Press: New York, 1981; Chapter 10.
(3) Perrin, A.; Sergent, M.; Fisher, Ø. *Mater. Res. Bull.* **1978**, *13*, 259.
(4) Perrin, A.; Chevrel, R.; Sergent, M.; Fischer, Ø. *J. Solid State Chem.* **1980**, *33*, 43–47.

0002-7863/83/1505-1150$01.50/0 © 1983 American Chemical Society